

Ultrafast Surface Plasmonic Switch in Non-Plasmonic Metals

E. Bévilion,¹ J.P. Colombier,^{1,*} V. Recoules,² H. Zhang,¹ C. Li,¹ and R. Stoian¹

¹*Laboratoire Hubert Curien, UMR CNRS 5516, Université de Lyon,
Université Jean-Monnet, 42000 Saint-Etienne, France*

²*CEA-DIF, 91297 Arpajon, France*

(Dated: September 11, 2015)

We demonstrate that ultrafast carrier excitation can drastically affect electronic structures and induce brief surface plasmonic response in non-plasmonic metals, potentially creating a plasmonic switch. Using first-principles molecular dynamics and Kubo-Greenwood formalism for laser-excited tungsten we show that carrier heating mobilizes d electrons into collective inter and intraband transitions leading to a sign flip in the imaginary optical conductivity, activating plasmonic properties for the initial non-plasmonic phase. The drive for the optical evolution can be visualized as an increasingly damped quasi-resonance at visible frequencies for pumping carriers across a chemical potential located in a d -band pseudo-gap with energy-dependent degree of occupation. The subsequent evolution of optical indices for the excited material is confirmed by time-resolved ultrafast ellipsometry. The large optical tunability extends the existence spectral domain of surface plasmons in ranges typically claimed in laser self-organized nanostructuring. Non-equilibrium heating is thus a strong factor for engineering optical control of evanescent excitation waves, particularly important in laser nanostructuring strategies.

I. INTRODUCTION

Collective non-equilibrium effects on transport properties in metallic systems are topics of current interest as non-standard behaviors play an increasing role in optics, thermodynamics or magnetism. Ultrafast laser electronic heating can mobilize localized states, inducing massive nonlinear contributions to optical and thermal transport or structural metastability. Understanding the intimate electronic mechanisms of optical coupling in excited solids and controlling excitation transients is therefore of prime importance as new applications are emerging in ultrafast optics, plasmonics and heat control strategies. If consequences for transport are readily expectable [1, 2], and the role of nonequilibrium electronic transfer was early recognized [3, 4], subtle atomistic effects can be inferred at the level of the band structure with unexpectedly strong consequences. Charge transfer and screening during non-equilibrium concur to a dynamic self-adjustment of thermal and optical properties to accommodate swift excitation. Recoules *et al.* [5] proved that participation of localized d orbitals in noble metals enforces the lattice cohesion. Non-equilibrium charge supply allows large variations of thermal characteristics in transition metals [6], fluidifying energy transport [7]. Non-thermal distributions can restrict the collisional phase-space around the Fermi level, severely damping electron-phonon coupling [8]. Furthermore, electronic occupation of delocalized states and filling from localized reservoirs (e.g. d -bands in transition metals) redefine classical views on free electron density [9], introducing significant dynamics in optical behaviors. Tuning ultrafast optical response via electronic reactions was thus

proposed for active large bandwidth modulation in ultrafast plasmonics [10]. Engineering macroscopic optical response on ultrafast scales equally relates to the onset of optical resonances [11, 12] on excited surfaces with spectral and spatial disturbances, e.g. Wood's anomalies. One debated example concerns ultrafast laser nanostructuring of solids in self-assembled regular patterns. The universal phenomenon - observed half a century ago [13] - carries application potential in functional surfaces [14], color-coded optical traceability and multidimensional information storage [15, 16], or feedback-driven nanolithography [17]. Key questions in laser-induced periodic surface structures (LIPSS) concern the origin of spatially-modulated energy patterns [18] and the interplay between optical resonances and nonlinear feedback. Electromagnetic calculations indicate the involvement of surface waves inducing collective motion [18]. Among them, surface plasmon (SP) with its ability to enhance electromagnetic energy on nanoscales holds a determinant role.

The potential involvement of SPs interference in laser nanostructuring is in close relation to surface optical indices. Thus the experimentally-observed onset of polarization-dependent periodic structures for non-plasmonic metals, as demonstrated on tungsten [19], is intriguing in optical ranges theoretically forbidden by predictions based on ambient optical indices. A typical example of ultrafast LIPSS at 800 nm is provided in Fig. 1(a), showing quasi-wavelength periodicity. The positive real permittivity of W precludes normally the generation of electronic surface waves and plasmon polariton coupling. The possibility to excite collective material motion pinpoints to a more intricate dynamic response of the system. We investigate the impact of ultrafast heating on electronic structures capable of initiating a large excursion of optical properties, namely an excitation-driven plasmonic state in otherwise non-plasmonic solid non-Drude-like metal. First-principles

* jean.philippe.colombier@univ-st-etienne.fr

approaches are chosen to interrogate electronic-driven evolution of optical properties and their consequences on plasmonic behaviors at time and spatial scales difficultly accessible by experiments.

II. CALCULATION DETAILS

The calculations correspond to ultrashort pulse irradiation conditions enabling LIPSS around the damage threshold (90 mJ cm^{-2} absorbed fluence). Transient electron and lattice temperatures in W for single ultrashort pulse irradiation (Fig. 1(b)) are estimated using a two-temperature hydrodynamic code (Esther) [20] which describes the energy balance using Helmholtz optical formalism and electron-phonon relaxation with temperature-dependent transport properties [6, 9]. Electronic temperatures on the rising heat cycle can amount to $2.5 \times 10^4 \text{ K}$, inducing electron-phonon nonequilibrium up to 3 ps, with the material in solid state for at least 1 ps. Internal electronic thermalization is assumed, justified by high levels of energy deposition in the vicinity of the threshold which accelerates electronic energy exchange to fs scales [8]. In this range, calculations are carried out with the plane-wave code Abinit [21], in the frame of the density functional theory [22, 23] extended to finite electronic temperatures [24]. The generalized gradient approximation [25] is employed to model exchange and correlation energies, and projector augmented-waves atomic data [26] account for the effects of nuclei and core electrons. A 54 atoms supercell of body centered cubic (bcc) W is considered, with $5s^25p^65d^46s^2$ valence electronic configuration; $4f$ electrons are neglected as their effect is weak at the T_e considered here [9]. We first perform *ab initio* molecular dynamics simulations in the isokinetic ensemble at room temperature, with $T_i = T_e = 300 \text{ K}$ during 2 ps. This calculation provides an average thermodynamic equilibrium from which ionic configurations are extracted, standing for representative states of the W lattice at ambient conditions. Then electronic structures are computed at T_e of 300, 10^4 and $2.5 \times 10^4 \text{ K}$. They serve as a basis to evaluate optical properties in solid phase at these levels of electronic excitation.

III. RESULTS

We first focus on the evolution of the electronic density of states (DOS) with electronic temperatures in the presence of a cold, ambient lattice, with calculated DOS profiles provided in Fig. 1(c). If finite ionic temperature induces a certain smoothing of the features compared to calculations at $T_i = 0 \text{ K}$ [9] due to a loss of degeneracy arising from atom oscillations around their high symmetry position, a highly-structured d band remains. The DOS shape is remarkably stable against electronic heating with a maximal d block shift of 0.15 eV at $2.5 \times 10^4 \text{ K}$, indicative of a stiff electronic structure. This

relates to the roughly symmetric profile of the DOS on both sides of the electronic chemical potential μ . The high density of empty electronic states on the right side of the Fermi level collects the excited electrons from the left-sided filled electronic states, leading to a weak T_e dependence of μ , contrary to most of transition metals [6, 9]. The location of the chemical potential within a mid-range pseudo-gap between high density of filled and empty electronic states determines the non-plasmonic behavior in the 1-5 eV range, i.e. for visible photon energies bridging the gap. The increase of T_e determines however a slight augmentation of the number of d electrons from low-lying part of sp orbitals, implying a moderately strengthen localization of the charge density, noted in increasing Hartree energies [9]. The main T_e effect resumes to a Fermi broadening within the DOS. The impact of the occupation probability is discussed below.

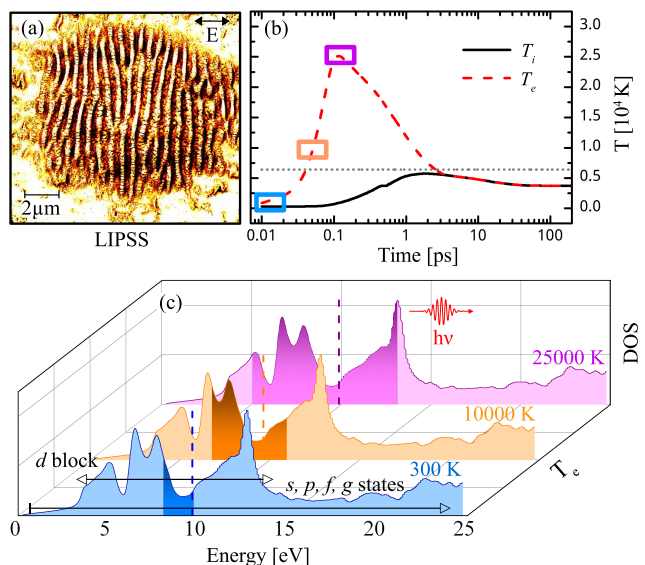


FIG. 1. (Color online) (a) Typical field-perpendicular surface periodic nanostructures at quasi-wavelength periodicity induced by 800 nm 50 fs laser pulses on W. (b) Electron (dashed red) and lattice (solid black) temperature evolutions for W irradiated by a 50 fs laser pulse. Dotted line indicates the standard vaporization limit. (c) DOS of bcc W computed at $T_i = 300 \text{ K}$ and its evolution with T_e . Dashed lines indicate the Fermi levels and dark colored areas show occupied electronic states mainly impacted by 800 nm photons.

Relying on the as determined electronic structures, the subsequent optical properties are obtained from an average on three ionic configurations. The real part of the frequency-dependent optical conductivity is obtained within the Kubo-Greenwood (KG) formalism [27]:

$$\sigma_r(\omega) = \frac{2\pi}{3\omega\Omega} \sum_{i,j,k} \sum_{\alpha=1}^3 [f(\epsilon_{i,k}) - f(\epsilon_{j,k})] \times |\langle \Psi_{j,k} | \nabla_{\alpha} | \Psi_{i,k} \rangle|^2 \delta(\epsilon_{j,k} - \epsilon_{i,k} - \hbar\omega), \quad (1)$$

where electronic transitions from i to j states are integrated over the reciprocal space for each photon energy $\hbar\omega$, accounting for the Fermi-Dirac occupations $f(\epsilon)$ and the eigenenergies of the electronic states ϵ . ∇ represents the velocity operator. Ω is the volume of the cell while α corresponds to the three spatial dimensions. The imaginary part of the frequency-dependent conductivity is obtained using the Kramers-Kronig (KK) relation, $\sigma_i(\omega) = -\frac{2}{\pi} \mathcal{P} \int_0^\infty \frac{\sigma_r(\omega')\omega}{\omega'^2 - \omega^2} d\omega'$, where \mathcal{P} is the principal value of the integral. Frequency-dependent permittivities and optical indices can be derived.

Optical properties follow electronic structure evolutions and large excursions up to plasmonic states are argued below. Fig. 2 shows the computed frequency-dependent optical conductivities $\tilde{\sigma} = \sigma_r + i\sigma_i$ and optical indices $\tilde{n} = n + ik$ as a function of the electronic temperature. A good agreement is found between theoretical values obtained at 300 K and the reflectivity measurements of Weaver [28], confirming a realistic description of the W electronic structure. σ_r is an implicit measure of optical absorption and its spectral behavior can be inferred based on the profile of the energy bands calculated in Fig. 1(c). For the low T_e case (dotted blue line), at photon energies below 0.5 eV, the intraband part dominates, resulting from electronic transitions inside $6sp$ bands. This contribution rapidly decays as the photon energy increases. On the other hand, interband transitions originating from the partially filled $5d$ sub-bands become gradually more important [29]. From 0.5 to 5.1 eV, photon-driven electronic transitions access an increasingly larger DOS domain ($\pm\hbar\nu$) centered on μ , resulting in a stepwise build-up of $\sigma_r(\omega)$ mapping the local DOS. This trend can be seen as the wing slope of a resonant behavior around the 5.1 eV peak given by the particular electronic DOS splitting around the Fermi level and the finite width of the sidebands. The conductivity finally decreases once main d -bands peaks have been included and diluted into the continuously increasing electronic transition phase-space. From the KK relation, $\sigma_i(\omega)$ relies on the overall $\sigma_r(\omega)$ profile. Conceptually, this integral can be separated in two parts depending on the value of ω' with respect to the reference value ω . For $\omega' \in [0, \omega]$, the integral is negative and reverse signs for higher ω' . Accordingly, the magnitude of σ_i depends on the profile of the real conductivity mainly around ω . A quasi-symmetric profile of σ_r tends to balance positive and negative components of the integral and provide low values for σ_i . On the contrary, an asymmetric profile emphasizes the respective sign components of the integral, depending on the trend of asymmetry (left or right-turned), determining positive or negative values of the imaginary conductivity. For W, the positive slope of σ_r profile from 1 to 5.1 eV with values ranging from 0.5×10^4 to 1.7×10^4 S cm $^{-1}$ leads to a negative $\sigma_i(\omega)$ at ambient conditions. A spectral view on $\sigma_i(\omega)$ indicates an anomalous-like dispersive behavior related to the absorption resonances.

The profiles of optical conductivities in Fig. 2(a,b) and optical indices in Fig. 2(c,d) significantly change with

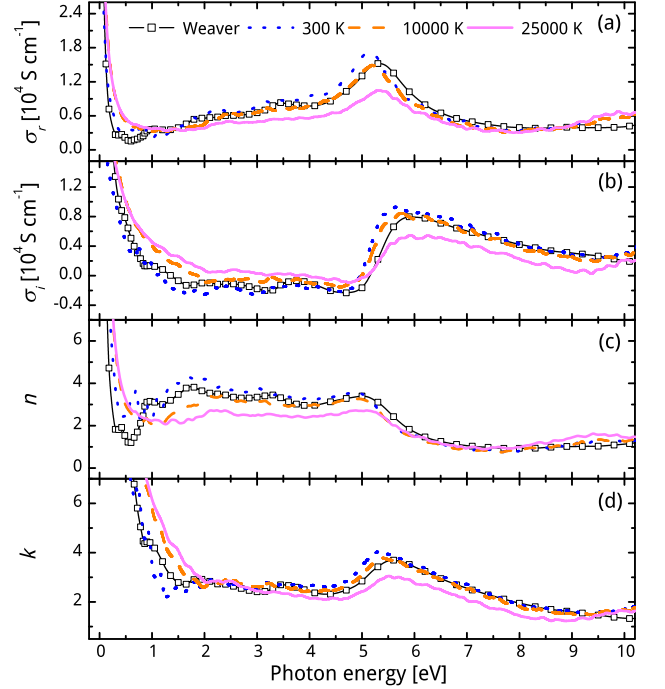


FIG. 2. (Color online) Real (a) and imaginary (b) part of the frequency-dependent optical conductivity; real (c) and imaginary (d) part of the optical indices. Colored curves stand for the electronic temperatures of 300 K, 10^4 K and 2.5×10^4 K and the squares represent the experimental data for non-excited W [28].

the electronic temperature, requiring an introspection in the corresponding excitation-driven electronic effects. If the observed changes in optical properties are not a consequence of DOS variation due to its stability against heating, the electronic temperature affects the degree of filling. Thus the optical evolution is the direct consequence of a broadened Fermi-Dirac charge redistribution, making more states available for photon-induced transitions. With the increase of T_e , the optical transitions concern an increasing μ -centered interval mainly corresponding to $[-\hbar\nu - \frac{3}{2}kT_e, \hbar\nu + \frac{3}{2}kT_e]$ [30], illustrated in Fig. 1(c) for a photon energy of 1.55 eV. The consequence is manifold, observable in the σ_r which maps the spectral absorption. Firstly this produces a broadening of available transition phase-space for the various photon energies. This translates into an increase of the intraband part, balanced by a decrease in the interband domain (qualitatively similar to a clockwise turn), damping the σ_r 5.1 eV peak. The subsequent asymmetric change of slope in σ_r with T_e determines the increase of σ_i in the 1-5 eV (as the dispersive behavior across the resonance flattens) and a passage in the positive values domain for a significant part of the spectral domain. The situation becomes more clear in the evolution of the optical indices. At 1.55 eV (800 nm), relevant for the LIPSS, optical indices are strongly affected by the heating of the

electronic system, with $\tilde{n} = 4.0 + 2.4i$ at 3×10^2 K reaching $\tilde{n} = 2.1 + 3.8i$ at 2.5×10^4 K. Thus, in the near infrared and low frequency visible part of the spectrum, the real part of the index goes down and the imaginary part augments.

IV. EXPERIMENTAL CONFIRMATION

The evolution was confirmed by time-resolved pump-probe ultrafast ellipsometry on laser-excited W surfaces. The transient optical properties upon ultrafast (120 fs) laser irradiation were probed at 1.55 eV photon energy using a two-angle one color time-resolved ellipsometry method following the technique proposed in Ref. [31]. The static properties of the non-excited surface were first evaluated ex-situ using a commercial ellipsometer (Uvisel, Horiba Jobin Yvon) and the results give $\tilde{n} = 3.57 + i3.15$ for massive W materials (Goodfellow 99.95% purity, mechanically polished). Alongside massive W, foils (Goodfellow 0.3 mm thick, polished at 0.1 mRa -purity 99.95%) were equally used as reference. The dynamic reflectivity changes were subsequently interrogated on massive thick targets by p-polarized 120 fs, 800 nm low energy non-perturbing probe laser pulses at 27.1° and 65.8° incidence angles. The probe pulses were time-synchronized with fs accuracy with the exciting pump pulse of equally 120 fs 800 nm, arriving at normal incidence on the W surface. Two photodiode detectors were used in imaging geometries with respect to the surface. The probed zone is significantly smaller than the spatial extent of the excited region. The exciting fluences were chosen slightly below the ablation threshold.

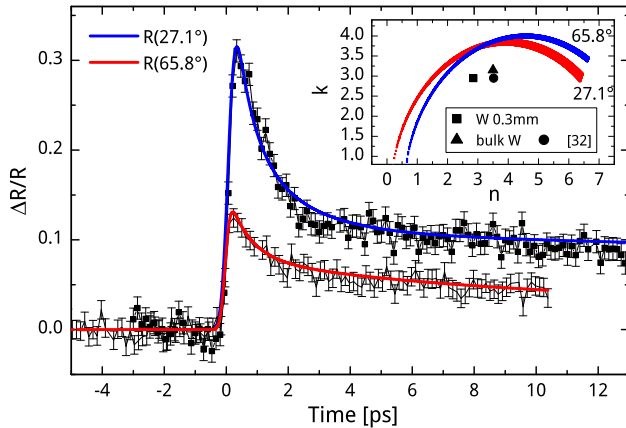


FIG. 3. (Color online) Example of dynamic time-resolved reflectivity traces at the two probe angles (27.1° and 65.8°) at incident pump peak fluence of 0.12 J/cm^2 . Inset: (n, k) contour plots corresponding to measured reflectivities at the two given angles. The intersection point represents a uniquely determined (n, k) pair satisfying simultaneously the two reflectivity conditions. Non-excited values obtained from ellipsometric measurements on bulk and foil samples as well as literature data [32] are given as references.

The swift optical activity on massive W samples is underlined by strong reflectivity changes, with a reflectivity snapshot example for an input peak fluence of 0.12 J/cm^2 , just below damage threshold being shown in the Fig. 3 (a). The time-profile of the reflectivity transients maps the heating/cooling cycle of the electronic system and the associated redistribution in the electronic occupation around the chemical potential with T_e . The measured maximum values of the transient reflectivity changes occurring just after the peak of the excitation pulse were then depicted in terms of corresponding (n, k) values in the (n, k) optical phase-space. They represent uniquely-determined (n, k) pairs obtained by inverting Fresnel formulas at the given angles. The result is presented in Fig. 3 (b). The intersection point of the (n, k) contour plots corresponding to two angle-resolved measured reflectivities were used to extract the corresponding (n, k) pair, allowing thus access to the evolution of optical indices. The result is $\tilde{n} = 3.21 + i3.77$, where resulting optical indices indicate slight n decrease and increase in k above the experimental value of its dispersive part. Note that these correspond to a macroscopic state averaged over a region set by the optical penetration depth of 18 nm, with inhomogeneous temperature distribution. The accuracy of the measurement is affected by the roughness and local planarity of the surface and care was taken to minimize the errors. The optical evolution has strong impact on the possibility to excite surface plasmon, with the fulfilment of the required optical conditions.

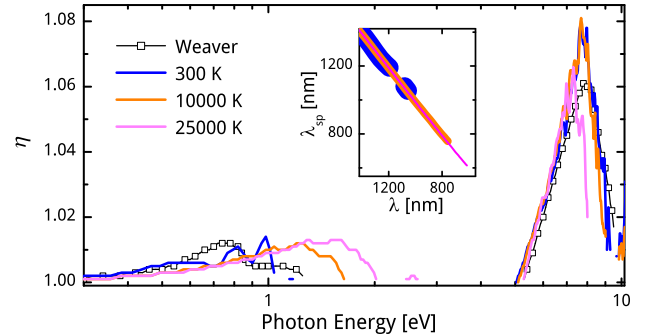


FIG. 4. (Color online) Real part of the effective refractive indices (η) in case of air-tungsten interface as a function of T_e . The symbol line stands for experimental data. Inset: variation of plasmon wavelength as a function of laser wavelength in a spectral domain ranging from 0.9 to 2.3 eV.

For air-material interfaces the condition for surface plasmon existence reduces to $\epsilon_r = n^2 - k^2 < -1$, a condition fulfilled in the conditions of Fig. 3, marking thus the ultrafast plasmonic activation at fluencies in the close vicinity of the damage threshold.

V. DISCUSSION

Surface plasmon periodicity λ_{sp} as a function of laser wavelength λ is given by $\lambda_{sp} = \lambda/\eta$, where $\eta = \Re\{[\tilde{n}^2/(\tilde{n}^2 + 1)]^{1/2}\}$ is the real part of the effective refractive index [33]. Calculated η is plotted in Fig. 4 and the absence of data indicates non-existence domains of surface plasmons. With the increase of T_e , one can note the expansion of the existence domain in the red photon energy region. The temperature-induced broadening of the electronic transition domain determines thus a plasmonic switch at visible optical frequencies. It appears that, upon electronic excitation, the light-induced onset of plasmonic character can sustain an origin based on optical resonances for LIPSS at 800 nm even though room temperature optical indices indicate non-plasmonic properties. As expected for air-metal interfaces, η remains close to one, especially at low photon energy, leading to λ_{sp} slightly inferior to the laser wavelength (inset of Fig. 4).

From the expression of the dielectric permittivity $\tilde{\epsilon} = 1 + i\tilde{\sigma}/\omega\epsilon_0$ the existence condition can be expressed more directly in terms of imaginary conductivity (and implicitly on real permittivity) with $\sigma_i > 2\omega\epsilon_0$. To clarify processes leading to the increase of the existence domain, we propose a simplifying approach. The imaginary conductivity is tentatively split into intra and interband components as depicted in Fig. 5(a,b). We first compute optical properties for a degenerate electronic system at $T_i = 0$ K and $T_e = 300, 10^4$ and 2.5×10^4 K. This disregards ionic temperature and phonon effects, assuming they assist mostly the intraband component via momentum conservation conditions. Conceptually this is justified in a classical view by the temperature dependence of damping frequencies. Accordingly, the intraband contribution vanishes and $\sigma_i^{inter} \simeq \sigma_i(T_i = 0$ K) (Fig. 5(b)). The intraband part at $T_i = 300$ K is then extracted by subtracting the as-determined T_i -insensitive interband part from the total value of the imaginary conductivity (Fig. 2(b)). In the visible spectral range, the intraband part σ_i^{intra} rapidly increases with the rise of T_e and saturates at 10^4 K. An example of this behavior at 1.55 eV is given in the inset. At the opposite, the interband part shows a more complex behavior, with negative values of σ_i^{inter} in the 0 to 5 eV energy interval that leads to negative values of the total imaginary conductivity, explaining the non-plasmonic nature of this metal. At higher energies, a resonance-like dispersive shape induced by the 5.1 eV peak of σ_r is clearly visible (Fig. 5(b)). By weakening the peak of σ_r , Fermi broadening also flattens the shape of σ_i^{inter} around the resonance and gradually reduces its negative component, progressively switching on plasmonic properties of W. The increase is not yet saturated at 2.5×10^4 K giving the possibility of a stronger lift and a subsequent extension of the plasmon existence domain for higher electronic temperatures. This highlights the preponderant role of d -electron-driven interband transitions in the optical response at high T_e .

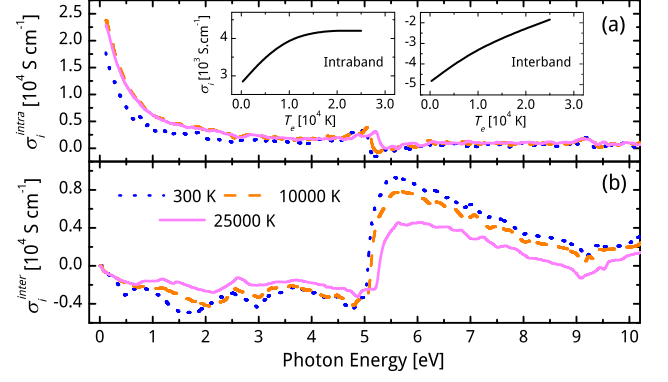


FIG. 5. (Color online) Intra and interband contribution to the imaginary conductivity as a function of T_e . Inset: Local evolution of $\sigma_i(T_e)$ at 1.55 eV.

The electronic evolution described above is related to the fast achievement of the non-equilibrium electron-lattice phase. However, W is a strong coupling material and lattice effects may be rapidly generating along the electronic relaxation. Performing simulations at different lattice temperature values we observe that a ionic temperature effect is indeed observable, increasing slightly the plasmon existence domain. This is attributed to a loosening of the atomic order initially responsible for the material non-plasmonic nature. However the effect is of secondary importance compared to the charge redistribution induced by the electronic temperature within the band structure. We conclude that lattice heating, albeit its influence on atomic order, does not severely impact the calculated electronic structure on the relevant timescales, maintaining a dominant electronic drive for the process.

VI. CONCLUSION

In conclusion, electron temperature dependent *ab initio* MD-KG calculations of solid state W indicate large duty-cycle optical tuning upon ultrafast laser irradiation and potential excitation of propagating collective electronic motion for an initially non-plasmonic state. We demonstrate that the evolution of optical properties with T_e produces, via the necessary optical conditions, an extension of the predictable existence domain of surface plasmon in the visible range, rendering possible a transient plasmonic phase and a potential plasmonic involvement in LIPSS. The necessary condition for optical indices was confirmed by time-resolved ellipsometry on excited W surfaces. The dynamic evolution mechanism is related to a redistribution of localized d -electrons across a chemical potential located in a d -band pseudo-gap. Since the DOS is not distorted by electronic heating, the changes of plasmon properties, indicated here by corresponding changes of optical conductivities, are prin-

cipally due to Fermi broadening within a structured d -block, extending the transition space for visible frequencies. By depopulating low-lying electronic states in favor of high electronic states, quasi-resonant transitions from regions of high DOS are diluted in a continuum of transitions. The dissimilar behaviors of intra and interband absorption events mark thus the evolution of the optical conductivity towards fulfilling resonant conditions. Similar phenomena may occur in other metals exhibiting non-plasmonic characteristics [32], especially Cr and Mo, as they crystallize in a similar structure. Stronger changes of optical properties [34] are to be expected in case of transition and noble metals where the electronic structure varies substantially with electronic temperature. All these effects have implications for optical tunability and

ultrafast switching of plasmonic properties extending beyond the domain of laser nanostructuring and validate concepts of structure engineering for metallic materials.

VII. ACKNOWLEDGMENTS

We thank N. Faure and M. Torrent for experimental and computing support. This work was supported by ANR project DYLPSS (ANR-12-IS04-0002-01) and by LABEX MANUTECH-SISE (ANR-10-LABX-0075) of the Université de Lyon, within the ANR program "Investissements d'Avenir" (ANR-11-IDEX-0007). Calculations used resources from GENCI (project gen7041).

-
- [1] M. P. Desjarlais, J. D. Kress, and L. A. Collins, "Electrical conductivity for warm, dense aluminum plasmas and liquids," *Phys. Rev. E* **66**, 025401 (2002).
 - [2] Z. Chen, B. Holst, S. E. Kirkwood, V. Sametoglu, *et al.*, "Evolution of ac Conductivity in Nonequilibrium Warm Dense Gold," *Phys. Rev. Lett.* **110**, 135001 (2013).
 - [3] H. E. Elsayed-Ali, T. B. Norris, M. A. Pessot, and G. A. Mourou, "Time-resolved observation of electron-phonon relaxation in copper," *Phys. Rev. Lett.* **58**, 1212 (1987).
 - [4] R. W. Schoenlein, W. Z. Lin, J. G. Fujimoto, and G. L. Eesley, "Femtosecond studies of nonequilibrium electronic processes in metals," *Phys. Rev. Lett.* **58**, 1680 (1987).
 - [5] V. Recoules, J. Cl  rouin, G. Z  rah, P. M. Anglade, and S. Mazevet, "Effect of Intense Laser Irradiation on the Lattice Stability of Semiconductors and Metals," *Phys. Rev. Lett.* **96**, 055503 (2006).
 - [6] Z. Lin, L. V. Zhigilei, and V. Celli, "Electron-phonon coupling and electron heat capacity of metals under conditions of strong electron-phonon nonequilibrium," *Phys. Rev. B* **77**, 075133 (2008).
 - [7] Y. V. Petrov, N. Inogamov, and K. Migdal, "Thermal conductivity and the electron-ion heat transfer coefficient in condensed media with a strongly excited electron subsystem," *JETP letters* **97**, 20 (2013).
 - [8] B. Y. Mueller and B. Rethfeld, "Relaxation dynamics in laser-excited metals under nonequilibrium conditions," *Phys. Rev. B* **87**, 035139 (2013).
 - [9] E. B  villon, J. P. Colombier, V. Recoules, and R. Stoian, "Free-electron properties of metals under ultrafast laser-induced electron-phonon nonequilibrium: A first-principles study," *Phys. Rev. B* **89**, 115117 (2014).
 - [10] K. F. MacDonald, Z. L. S  mson, M. I. Stockman, and N. I. Zheludev, "Ultrafast active plasmonics," *Nat. Photon.* **3**, 55 (2009).
 - [11] B. Luk'yanchuk, N. I. Zheludev, S. A. Maier, N. J. Halas, P. Nordlander, H. Giessen, and C. T. Chong, "The Fano resonance in plasmonic nanostructures and metamaterials," *Nat. Mater.* **9**, 707 (2010).
 - [12] A. Hessel and A. A. Oliner, "A New Theory of Wood's Anomalies on Optical Gratings," *Appl. Opt.* **4**, 1275 (1965).
 - [13] M. Birnbaum, "Semiconductor Surface Damage Produced by Ruby Lasers," *J. Appl. Phys.* **36**, 3688 (1965).
 - [14] V. Zorba, E. Stratakis, M. Barberoglou, E. Spanakis, P. Tzanetakis, S. H. Anastasiadis, and C. Fotakis, "Biomimetic Artificial Surfaces Quantitatively Reproduce the Water Repellency of a Lotus Leaf," *Adv. Mater.* **20**, 4049 (2008).
 - [15] B. Duss  r, Z. Sagan, H. Soder, N. Faure, J.-P. Colombier, M. Jourlin, and E. Audouard, "Controlled nanostructures formation by ultra fast laser pulses for color marking," *Optics express* **18**, 2913 (2010).
 - [16] J. Zhang, M. Gecevi  ius, M. Beresna, and P. G. Kazansky, "Seemingly Unlimited Lifetime Data Storage in Nanostructured Glass," *Phys. Rev. Lett.* **112**, 033901 (2014).
 - [17] B.   ktem, I. Pavlov, S. Ilday, H. Kalayciog  lu, *et al.*, "Nonlinear laser lithography for indefinitely large-area nanostructuring with femtosecond pulses," *Nat. Photon.* **7**, 897 (2013).
 - [18] J. E. Sipe, J. F. Young, J. S. Preston, and H. M. van Driel, "Laser-induced periodic surface structure. I. Theory," *Phys. Rev. B* **27**, 1141 (1983).
 - [19] A. Y. Vorobyev and C. Guo, "Femtosecond laser-induced periodic surface structure formation on tungsten," *Journal of Applied Physics* **104**, 063523 (2008).
 - [20] J.-P. Colombier, P. Combis, E. Audouard, and R. Stoian, "Guiding heat in laser ablation of metals on ultrafast timescales: an adaptive modeling approach on aluminum," *New Journal of Physics* **14**, 013039 (2012).
 - [21] X. Gonze, B. Amadon, P.-M. Anglade, J.-M. Beuken, *et al.*, "ABINIT: First-principles approach to material and nanosystem properties," *Computer Physics Communications* **180**, 2582 (2009).
 - [22] P. Hohenberg and W. Kohn, "Inhomogeneous Electron Gas," *Phys. Rev.* **136**, B864 (1964).
 - [23] W. Kohn and L. J. Sham, "Self-Consistent Equations Including Exchange and Correlation Effects," *Phys. Rev.* **140**, A1133 (1965).
 - [24] N. D. Mermin, "Thermal Properties of the Inhomogeneous Electron Gas," *Phys. Rev.* **137**, A1441 (1965).
 - [25] J. P. Perdew, K. Burke, and M. Ernzerhof, "Generalized Gradient Approximation Made Simple," *Phys. Rev. Lett.* **77**, 3865 (1996).

- [26] M. Torrent, F. Jollet, F. Bottin, G. Zérah, and X. Gonze, “Implementation of the projector augmented-wave method in the ABINIT code: Application to the study of iron under pressure,” *Comput. Mater. Sci.* **42**, 337 (2008).
- [27] S. Mazevet, M. Torrent, V. Recoules, and F. Jollet, “Calculations of the transport properties within the PAW formalism,” *High Energy Density Physics* **6**, 84 (2010).
- [28] J. H. Weaver, C. G. Olson, and D. W. Lynch, “Optical properties of crystalline tungsten,” *Phys. Rev. B* **12**, 1293 (1975).
- [29] P. Romaniello, P. L. de Boeij, F. Carbone, and D. van der Marel, “Optical properties of bcc transition metals in the range 0-40 eV,” *Phys. Rev. B* **73**, 075115 (2006).
- [30] P. E. Hopkins, J. C. Duda, J. L. Salaway, R. N. and Smoyer, and P. M. Norris, “Effects of Intra- and Interband Transitions on Electron-phonon Coupling and Electron Heat Capacity after Short-pulsed Laser Heating,” *Nanosc. Microsc. Therm.* **12**, 320 (2008).
- [31] C. A. D. Roeser, A. M.-T. Kim, J. P. Callan, L. Huang, E. N. Glezer, Y. Siegal, and E. Mazur, “Femtosecond time-resolved dielectric function measurements by dual-angle reflectometry,” *Rev. Sci. Instrum.* **74**, 3413 (2003).
- [32] A. D. Rakić, A. B. Djurišić, J. M. Elazar, and M. L. Majewski, “Optical properties of metallic films for vertical-cavity optoelectronic devices,” *Appl. Opt.* **37**, 5271 (1998).
- [33] J. M. Pitarke, V. M. Silkin, E. V. Chulkov, and P. M. Echenique, “Theory of surface plasmons and surface-plasmon polaritons,” *Rep. Prog. Phys.* **70**, 1 (2007).
- [34] F. Garrelie, J.-P. Colombier, F. Pigeon, S. Tonchev, *et al.*, “Evidence of surface plasmon resonance in ultrafast laser-induced ripples,” *Opt. Express* **19**, 9035 (2011).